forests

MDPI

Type of the Paper (Article)

Fluid-solid interaction for the nonlinear pressure-flux relationship of bordered pits in conifers

Xia Peng[1]*, Wu Yunjie[1], Song Wenlong[1], Xie Li[1], Jia Ziyi[1], Wang Xin[1] and Li Qionglin[2]

[1] School of Mechanical and Electrical Engineering, Northeast Forestry University, Harbin 150000, China.
[2] School of Civil Engineering, Southwest Jiaotong University, Chengdu 610000, China
* Correspondence: xiapeng@nefu.edu.cn

Abstract:

The nonlinear pressure-flux relationship in conifer xylem was attribute to the fluid-solid interaction within bordered pit. However, there was a lack of comprehensive understanding regarding the fluid-solid interactions between the torus-margo structure and the water flow within the pit. A fluid-solid interaction model was developed including the elastic deformation of the torus-margo structure and the flow of water transportation. Nine pit samples were reconstructed using transmission electron microscopy (TEM) and scanning electron microscopy (SEM) pictures in order to develop fluid-solid coupling models for pits in stems of Platycladus orientalis. The deflection of the torus was roughly proportional to the pressure difference between tracheids, while the flow resistance exhibited a considerable non-linear increase. The pit resistance decreased and the pit ability to regulate water flow enhanced when the pit diameter increased. Both the pit resistance and the pit ability to regulate water decreased when the pit depth increased. The decrease of the Young's modulus for the margo promoted the non-linear pressure-flux relationship in bordered pits. The findings presented in this work provided theoretical support for the non-linear relationship between pressure and flux in the bordered pit, as well as for the prevention of gas bubble transit through the bordered pit during tracheid cavitation.

Keywords: bordered pit; torus; pressure-flux; fluid-solid interaction; Platycladus orientalis

1. Introduction

The water transport in the xylem of coniferous trees was dependent on the efficacy of tracheids and bordered pits[1-3]. When comparing tracheids which had a short conduit-like appearance, the structure of bordered pits which possessed a centrally thickened region called the torus, as well as a porous region with radiating threads known as the margo has been recognized as a significant evolutionary trait that facilitated the transfer of water and prevented the spread of embolism[4,5]. With the presence of minuscule pores in the margo, it had been suggested that the bordered pits contributed more than half of the overall flow resistance in the xylem[6-8]. Furthermore, the torus, which was elastically supported by the margo, would experience deflection due to the pressure difference between tracheids[9]. The torus deflection could regulate flow rate during high flow rates or even close pits under high pressure, which was the so-called valve effect[10,11]. The passive valve effect in the bordered pit was characterized by the interaction between water flow and the torus-margo structure, as observed from a physical standpoint. However, there was to be a deficiency in comprehending the intricacies of fluid-solid interaction and its impact on the functionality of bordered pits.

To prevent gas bubbles from flowing out of tracheids, the aspiration of the bordered pit has been widely evidenced in the microscopic observation of samples collected from living trees[12-14], particularly after severe drought. In a microscopic experiment conducted by Mayr et al. on *Juniperus virginiana L*[15], the researchers studied the movement of air bubbles within tracheids and noted that gas bubbles were obstructed by the

Citation: To be added by editorial staff during production.

Academic Editor: Firstname Lastname

Received: date
Revised: date
Accepted: date
Published: date

Copyright: © 2023 by the authors. Submitted for possible open access publication under the terms and conditions of the Creative Commons Attribution (CC BY) license (https://creativecommons.org/licenses/by/4.0/).

presence of bordered pits. According to Savidge [16], bordered-pit structures have the potential to function as swinging-diaphragm check valves, controlling the movement of sap between adjacent tracheids. The study on stem hydraulic conductivity [17] revealed that there was a notable decrease in conductivity in conifer stems, specifically *Abies balsamea* and *Juniperus virginiana*, as the applied pressure increased. In contrast, the stem of the angiosperm *Acer saccharum* was observed to be almost unaffected by variations in pressure. The pressure difference required for the closure of the pits was found to be 0.0564 MPa for *Abies balsamea* and 0.075 MPa for *Juniperus virginiana*. In the study[18], similar findings were observed, indicating that the conductivity of coniferous stems, such as *Pinus sylvestris*, *Picea sitchensis*, and *Cedrus atlantica*, was influenced by the pressure gradient. However, the stem conductivity of angiosperms, such as *Fagus sylvatica*, was not reliant on the pressure gradient. Domec et al.[19]conducted measurements of specific conductivity in six different woody species, which included three conifers namely *Thuja plicata*, *Pseudotsuga menziesii*, and *Tsuga heterophylla*. The findings of the expriment demonstrated a non-linear relationship between sap flux and the pressure gradient in the xylem. As discussed in the studies[17-19], the results supported that the deflection of the torus elastically suspended by the margo could passively regulate the hydraulic conductivity in the bordered pit. In a microscopical mechanics study for bordered pits in *Pinus strobus* and *Larix laricinia*[20], the torus deflection from the margo stretching necessitated a far lower force for pit closure than initially anticipated. The experiment had difficulties in precisely measuring the force due to its magnitude being far lower than the noise level (3μN) of the force sensor. The results directly demonstrated the extreme compliance of the margo and confirmed the torus deflection when subjected to an external force. As the transpiration pull, which propelled water movement in the xylem of live trees, exhibited variability in response to environmental conditions[21], the significance of the nonlinear relationship between the pressure gradient in the xylem and sap flow rate was crucial in understanding the regulation of transpiration and photosynthesis [22]. As the microscopic measurement of both the flow rate and hydro force in the bordered pit was not feasible, there was a lack of reported information regarding the impact of pit geometry on torus deflection and hydraulic conductivity. Therefore, it was important to investigate the mechanism of the fluid-solid interaction and the nonlinear pressure-flux relationship in the bordered pit.

As the direct measurement of the hydraulic conductivity in bordered pits was very difficult, employing modeling techniques to simulate water flow within these structures emerged as a viable alternative. Lancashire and Ennos[23] utilized a scale approach to predict the hydraulic resistance based on the experimental flow results obtained from a macroscopically scaled artificial model of bordered pits. The lattice-Boltzmann method (LBM) was introduced by Valli et al. [24] for the purpose of simulating the flow in bordered pits, where the margo was treated as an isotropic porous material. The primary challenge in modeling the flow within bordered pits was the intricate and irregular structure of the margo. The oversimplification in the studies could not be rectified without the inclusion of empirical data from experiments. To avoid the oversimplifications, Schulte[25] employed computational fluid dynamics (CFD) technology to accurately simulate the complex morphology of the pores in the margo. This approach involved numerically solving the Navier-Stokes equation, which served as the fundamental governing equation for variable flows occurring in natural and engineering systems. The findings indicated that the flow through each pore in the margo was significantly influenced by the size of the pore area, as well as its radial position relative to the torus edge. Schulte et al. [26] further conducted a comparative analysis of the hydraulic characteristics of bordered pits in the stems and roots of *Picea mariana* and *Picea glauca*. The findings of the study suggested that the resistance to flow in pits located in roots was comparatively lower than that in pits located in stems. This disparity in resistance could be attributed to the greater dimensions of the pits in roots, as well as the presence of a margo with a bigger surface area in the pores. The computational fluid dynamics approach, implemented using commonly

standard software, offered a well-accepted way for calculating sap flow within bordered pits. Nevertheless, the investigations solely concentrated on the flow characteristics when the torus was positioned at the center, disregarding the potential influence of torus deflection. Therefore, it was important to develop a comprehensive model that integrated torus defection resulting from the deformation of the torus-margo structure.

To investigate the deflection of the torus when subjected to an external force, the utilization of mechanical analysis has developed as a prominent methodology. Sperry and Hacke [27] proposed a linear stress-strain model to assess the displacement of the pit membrane in angiosperm vessels under a pressure difference. Tixier et al. [28] provided a mechanical model that incorporated the geometric properties of the pits, based on the Kirchhoff-Love thin plate theory. When comparing the pit membrane in angiosperms to the torus-margo structure of pits in conifers, it was evident that the latter displayed a greater degree of intricacy. Hacke et al. [29] created a linear elastic model to predict torus deflection using a simplified margo structure that comprised a regular distribution of spokes. In order to effectively describe the torus-margo structure, Schulte et al. [30] utilized the finite element method (FEM) to construct an element discrete model, which directly incorporated the intricate geometry structure observed by electron microscopy. The investigation focused on the deflection of the torus caused by external forces and the stretching of the margo. The findings enhanced the understanding of the torus-margo structure in the process of pit closure. Peng et al. [31] elucidated the development of the contact seal in aspirated bordered pits by incorporating the contact behavior between the torus and the pit border into the FEM model. The findings indicated that the aspiration in bordered pits was influenced by the structural and material properties of the torus and margo. The standard FEM method with standard software provided a standard tool of modeling the structural deformation in bordered pits. With the assumption that the pressure difference on the torus-margo structure was uniformly distributed and to be a constant independent of the torus deflection, however, the external force would results in inevitable errors which were discussed in the study[30,31]. In bordered pit, the phenomenon of torus deflection was inherently attributed to the fluid-solid interaction between the torus-margo sturuture and the water flow. The water flow applied pressure forces on the torus-margo structure, resulting in torus deflection, while the structure, in turn, influenced the geometry of water flow field. Therefore, it was necessary to developed the fluid-solid interaction model to fully investigate the hydraulic features of bordered pits.

In the present study, a fluid-solid interaction model was developed to investigate the nonlinear pressure-flux relationship of bordered pits. This model focused on the interaction between the tours-margo structure and the water flow inside the bordered pits. The study revealed the interaction characteristics of how the torus deflected when the flow resistance was passively regulated under a pressure difference between tracheids. The study investigated the impact of the anatomical structure of bordered pits in the stem of *Platycladus orientalis* on the pressure-flux relationship. The results offered theoretical supports for the non-linear passive regulation of flow efficiency in bordered pit and would be useful for future studies on the phenomenon of pit aspiration when cavitation happened in tracheid.

2. Materials and Methods

2.1 The theory for fluid mechanics

The water flow in conifers' bordered pits could be characterized as a continuous flow, where the flow properties, such as water pressure and velocities, exhibited continuous variations within the flow field. This was due to the fact that the molecular free path of liquid water, which was approximately 3×10^{-4}μm[25], was significantly smaller than the microstructures in the bordered pit, which were larger than 1×10^{-3}μm. In the context of continuous flow, the Navier-Stokes equation was known as the fundamental set of equations that regulated laminar flow in natural. These equations represented the balance of

forces between external pressure, viscous shear forces inside the fluid, and fluid inertia[32].

In the study, it was assumed that the density of water within bordered pits remained constant and unaffected by pressure variations. Furthermore, it was assumed that temperature variation within the bordered pits was insignificant and the viscosity of the water remained constant. The equation governing momentum conservation for steady-state laminar flow with incompressible water and constant fluid viscosity could be expressed as follows:

$$\rho(\mathbf{V}\cdot\nabla\mathbf{V}) = -\nabla p + \mu\nabla^2\mathbf{V} \quad (1)$$

Where **V** is velocity rector(m/s), p is pressure(Pa), μ is fluid dynamic viscosity(Pa·s), and ρ is fluid density(kg/m3).

To resolve the momentum equation, it was necessary to incorporate the continuity equation to ensure the closure of fluid variables.

$$\nabla\mathbf{V} = 0 \quad (2)$$

Due to the unavailability of analytic solutions for the three-dimensional flow with complex geometry in bordered pits, the finite volume method (FVM) was employed to numerically solve the partial differential Navier-Stokes equations[33]. The process of constructing the FVM model typically involved three key steps including preparing fluid model, defining fluid properties, and applying pressure boundary.

2.2 The theory for solid mechanics

When the margo and the torus deformed under the fluid pressure, the mechanic equation of the elastic materials for the torus and the margo was[34],

$$0 = \boldsymbol{\sigma} + \mathbf{f} \quad (3)$$

Where **σ** is the internal stress induced by the material elastic deformation, and **f** is the external stress induced by the fluid pressure.

Hook's law was developed to describe the relationship between the stress (**σ**) and the strain (ε). Within the elastic limit of the material, the strain was proportional to the stress,

$$\boldsymbol{\sigma} = \mathbf{D}\boldsymbol{\varepsilon} \quad (4)$$

Where **D** was the matrix of the material which depended on the elastic modulus E and Poisson's ratio ν of the material.

For a complicated structure, the partial differential equations were solved by the finite element method (FEM) [35]. The development of the FEM model generally included preparing solid model, defining material properties, and applying external pressure and fixed constraints.

2.3 Fluid-solid interaction

Fluid-solid interaction was a phenomenon that occurred when a fluid medium interacted with a deformable structure. In this interaction, the fluid applied pressure forces on the structure, resulting in its deformation, while the structure, in turn, influenced the geometry of the flow field. In the context of fluid-structure interaction in a steady-state scenario, the torus-margo structure's solid model was solved in conjunction with the fluid model. The fluid model provided the external fluid pressure within the bordered pit for the solid model, while the solid model provided the elastic deformation of the torus-margo structure for the fluid model. Through a series of iterative processes involving the fluid model and the solid model, a state of equilibrium was ultimately achieved in the fluid-solid system[36]. This equilibrium was established by the balancing of external fluid pressure, as predicted by the fluid model, and the elastic deformation, as predicted by the solid model. The development of the fluid-solid interaction included developing the fluid model, developing the solid model and establishing data transfer between the fluid model and the solid model.

2.4 Plant material

The bordered pits modeled in the present study were from Platycladus orientalis. Ten stems were selected from branches in five approximately 1 meter trees in a

greenhouse at the Northeast Forest University located in Harbin, China. (45°04′N, 127°42′E, elevation 120 m). The samples were observed under scanning electron microscope and transmission electron microscope. The processes for sample collection, sample observation and sample data were detailed in our previous study[31].

2.5 *Model development*

The process for developing the fluid-solid interaction model of bordered pits was depicted in Figure 4, including the geometric model, the fluid model, the solid model, the fluid-solid interface data transfer, and coupling iteration solution. The process of reconstructing the geometric model from the two-dimensional micrographs to the 3D geometry was detailed in the study[31].

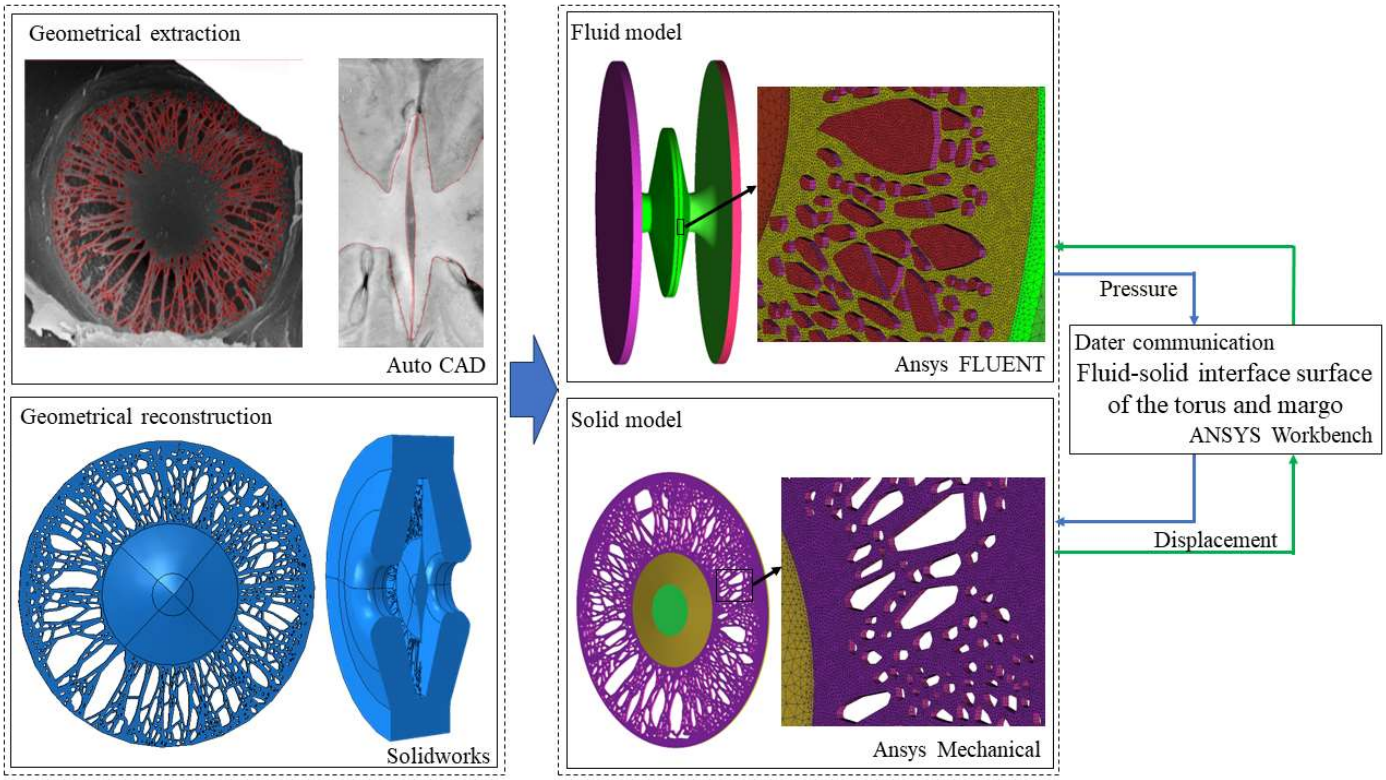

Figure 1. The process for developing the fluid-solid interaction model of bordered pits

To construct the fluid model, it was postulated that the flow field in bordered pits was fully filled with the pure water. The finite volume elements of tetrahedron in pit chamber and triangular prism in margo pores were used to discretize the 3D flow field. The quantity of the element in the bordered pit was about 6×10^6. The fluid model was developed in a commercial software Ansys FLUENT 2019 which was known for its advanced physics modeling capabilities and unmatched accuracy. In the simulation, the water density was 998 kg/m^3 and the water dynamic viscosity was 1.002×10^{-3}Pa·s (corresponding to water at 293.15K). The fluid velocity was assumed to be zero without any flow slip on the geometry boundaries like the torus, the margo, and the pit border. The pressure difference was applied on the upstream and downstream surface boundaries in tracheids.

To construct the solid model of the torus-margo structure, it was postulated in this preliminary study that the material property remained constant without nonlinear characteristics like material anisotropy, plastic, and yielding. The finite volume elements of triangular prism were used to discretize the 3D structures of the torus and the margo. The quantity of elements for the torus-margo structure was around 1.8×10^6. The simulation was performed using a commercial software Ansys Mechanical 2019, a widely used finite element program known for its ability to provide precise answers for nonlinear multi-

physics studies. According to the external force required for closing the stem pit was lower than 3μN[20], the elastic modulus was evaluated to be 0.3 GPa and the Poisson's ratio was selected to be 0.4.[31].

To transfer the displacement from the solid model to the fluid model meanwhile the pressure from the fluid model to the solid model, the software ANSYS workbench 2019 was used, which was an industry-standard interprocess communication tool between multi-physical fields. To prevent the data transfer errors, the surface elements on the interface surface between the fluid model and the solid model were necessary to use the same triangle surface elements with the overlap rate 100%. In the coupling solution, the fluid model firstly calculated the fluid pressure and velocities in flow field and transferred the pressure data on the interface to the solid model. With the fluid pressure, the solid model calculated the elastic deformation and transferred the displacement data on the interface to the fluid model. Then, the fluid model updated the geometry of the torus-margo structure with the interface displacement. With repeating the coupling computation, the coupling solution was obtained until the variations of the pressure and the displacement in a cycle should be lower than 0.1%. In each result, the water flowrate, the fluid pressure and velocity, and the deformation of the torus-margo structure were examined. The pit resistance was calculated from the model pressure difference divided by the volume flow through the model[25,26].

The simulations were conducted using a workstation equipped with an AMD 5995WX CPU and 256 GB of memory. The duration of the fluid-solid interaction simulation ranged from 15 to 41h, while the memory usage ranged from 130 to 160 GB. Furthermore, the statistical analysis of simulation results was conducted using standard functions within MATLAB version 2018a (MathWorks, Massachusetts, USA), a commonly employed programming and numeric computing platform for data analysis.

2.6 *Model verification*

The solid modeling and simulation technique was verified in our pervious study[31]. To verify the fluid model and the simulation technique, one of the bordered pits from the stem in the study[25] was reconstructed. The comparison in Table 1 showed that the present study had a good agreement with the Schulte's study. As the modeling deviation was inevitable in the manual reconstruction process, the maximum deviation between the studies was lower than 9.549%. Therefore, the flow modeling and simulation technique in the present study was reliable.

Table 1. The pit resistance verification of the components in bordered pits. The deviation between the present study and the study [25] as lower than 9.549%, as modeling errors were inevitable to manually create polygons for each pore in margo modeling.

	Pressure difference (Pa)	Resistance(Pa·s/m^3) in reference[2012]	Resistance(Pa·s/m^3) in present study	Derivation rate(%)
Canal	86.810	2.769×10^{15}	2.943×10^{15}	6.284
Torus and canal	292.000	9.302×10^{15}	9.875×10^{15}	6.160
Margo, torus and canal	473.400	1.508×10^{16}	1.652×10^{16}	9.549

3. Results

In our previous study[31], the data of stem bordered pits from Platycladus orientalis shown the positive correlation between the pit diameter and the torus diameter (p<0.001) and the negative relationship between pit diameter and pit depth (p=0.1171). Measured in the study, the total area of pores in the margo varied between 13.013μm^2 and 22.217μm^2 with an average area of 16.824 μm^2 and a standard deviation of 3.008μm^2. The positive relationship between pit diameter and total area of pores in the margo was significant (p<0.05).

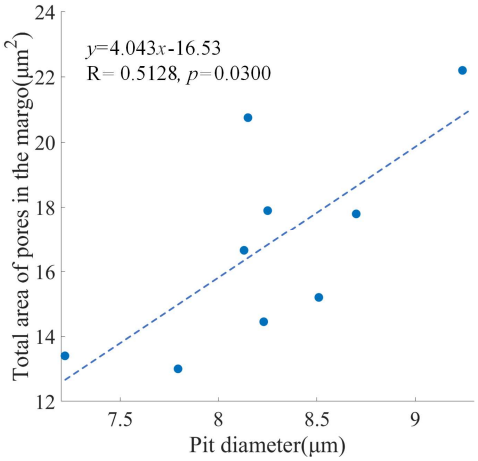

Figure 2. The total area of the pores in the margo measured in pit geometry model. The linear regression between the pit diameter and total area of pores in the margo was significant($p<0.05$).

When the torus was initially at the center position, Figure 3(a) illustrated the occurrence of pressure loss along the flow path within the bordered pit. Within the pit aperture and chamber, a pressure loss of averaged 9.564% was seen between probe A and C, as well as between probe H and J. Within the narrow gap between the torus-margo and pit border, the pressure loss between probe C and E, as well as between probe F and H, was averaged 17.185%. Across the margo, the pressure loss between probe C and H was 57.620%, while the pressure loss between probe D and G was 29.294% and the pressure loss between probe E and F was 23.251%. In figure 3(b), it was observed that the dimension and position of the pores in the margo had a significant impact on the velocity within each individual pore. The velocity observed in the larger pore was found to be greater than the velocity observed in the smaller pore. Specifically, the velocity measured at probe A (5.15mm/s) was higher than the velocity measured at probe D (4.12mm/s). The velocity observed in the pore located in adjacence of the torus was found to be greater than the velocity in the pore neighbor the margin of the pit membrane. For instance, the velocity measured at probe C (4.48 mm/s) exceeded the velocity measured at probe I(0.68mm/s).

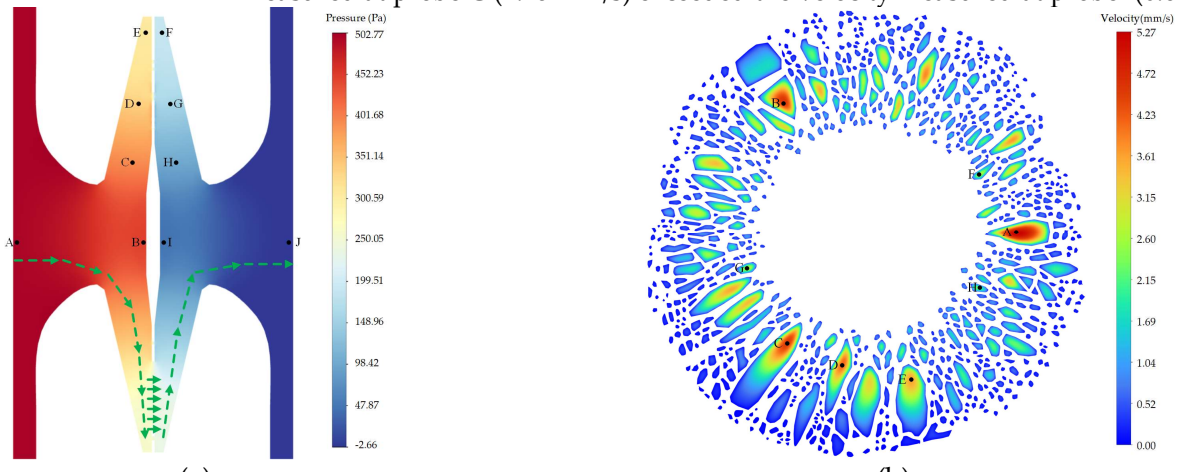

(a) (b)

Figure 3. The pressure and velocity in one of bordered pits with the torus placed at the center position. (a) Pressure distribution in the cross section, Probes (Pa) A:500, B:452.232, C:396.633, D:330.926, E:310.708, F:194.455, G:184.455, H:108.531, I:47.877, J:0. (b) Velocity distribution in the pores of the margo, Probes(mm/s) A:5.15, B:4.53, C:4.48, D:4.12, E:3.65, F:2.81, G:2.76, H:2.35, I: 0.68.

For the pit models with the torus placed at the center position, pit resistance varied between 3.6851×10^{16} and 6.5197×10^{16} Pa·s/m^3 with an average resistance of 4.7086×10^{16} Pa·s/m^3 and a standard deviation of 0.8242×10^{16} Pa·s/m^3. As depicted in Figure 4, a negative correlation was observed between the pit diameter and the pit resistance(p=0.3195) which , and a negative correlation was observed between the pit depth and the pit resistance(p=0.8307).

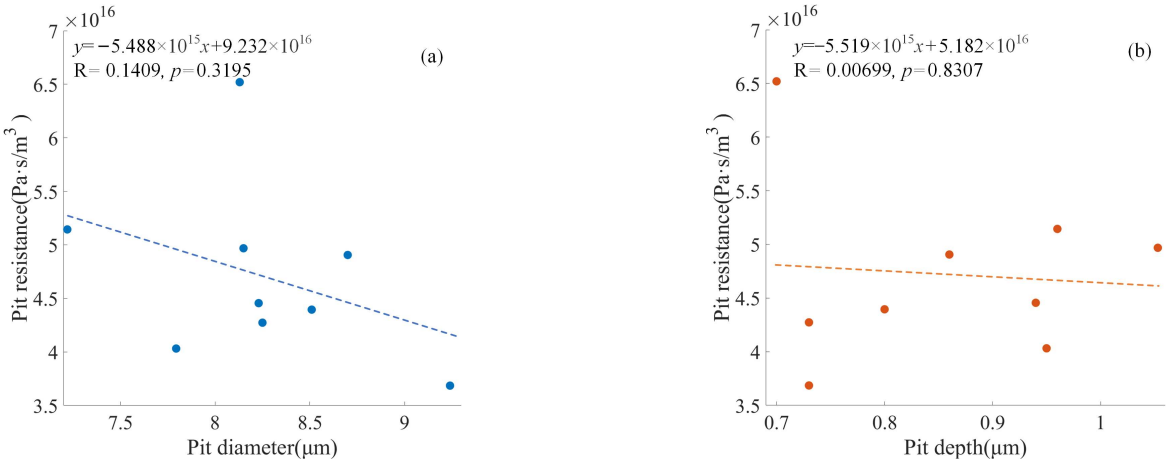

Figure 4. The influences of the pit diameter and the pit depth on the pit resistance with the torus at the initially center position. (a)The linear regression between the pit diameter and pit resistance(p=0.3195). (b) The linear regression between the pit depth and pit resistance(p=0.8307).

As depicted in Figure 5, fluid force on the torus varied between 2.388×10^{-3}μN and 5.207×10^{-3} μN with an average force of 3.699×10^{-3} μN and a standard deviation of 1.018×10^{-3} μN. The positive relationship between the fluid force on the torus and the torus diameter was very significant(p<0.05). Fluid force on the margo varied between 1.906×10^{-3}μN and 4.044×10^{-3}μN with an average area of 2.706×10^{-3}μN and a standard deviation of 0.718×10^{-3}μN. The positive relationship between the fluid force on the margo and the margo diameter was not significant(p=0.2335), as the pores were highly variable in the margo. Fluid force on the pit membrane varied between 4.324×10^{-3}μN and 8.489×10^{-3}μN with an average force of 6.406×10^{-3}μN and a standard deviation of 1.405×10^{-3} μN. The positive relationship between the fluid force on the pit membrane and the pit diameter was significant(p<0.1).

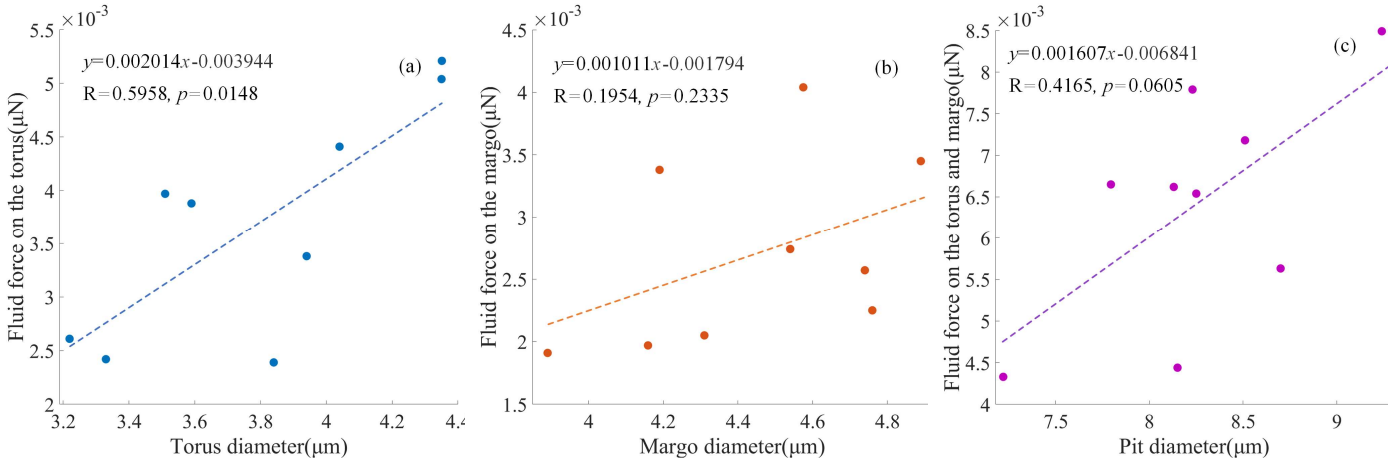

Figure 5. The influences of the torus diameter, margo diameter and pit diameter on the fluid forces with the torus at the initially center position. (a)the line regression between

torus diameter and force on the torus. (p<0.05) (b)the line regression between margo diameter and force on the margo.(p=0.2335) (c)the line regression between pit diameter and force on the torus and margo.(p<0.1)

The fluid-solid interaction, as depicted in Figure 6, resulted in the expansion of the upstream pit chamber and the narrow gap due to the torus deflection. Conversely, the downstream pit chamber and the narrow gap were shrunk. The act of stretching the margo resulted in the expansion of the pores within the margo. The alteration of the flow resistance in the flow path caused by the deformation of the torus and margo resulted in a corresponding alteration of the pressure loss within the bordered pit. The torus deflection resulted in a decrease in pressure variation in the upstream chamber and the narrow up, while causing a considerable increase in pressure fluctuation in the downstream narrow gap. According to the data presented in Figure 9, it can be observed that as the pressure difference grew from 500 to 1500Pa, the relative pressure loss in the downstream gap between the probe G and H exhibited an increase from 23.220 to 43.547%. Conversely, the relative loss across the margo between the probe D and G demonstrated a drop from 29.278 to 15.194%. The fluctuation in flow resistance, particularly at the downstream gap, led to a significant increase in flow velocity within the pore adjacent to the torus, compared to the flow velocity in the pore neighboring the margin of the pit membrane.

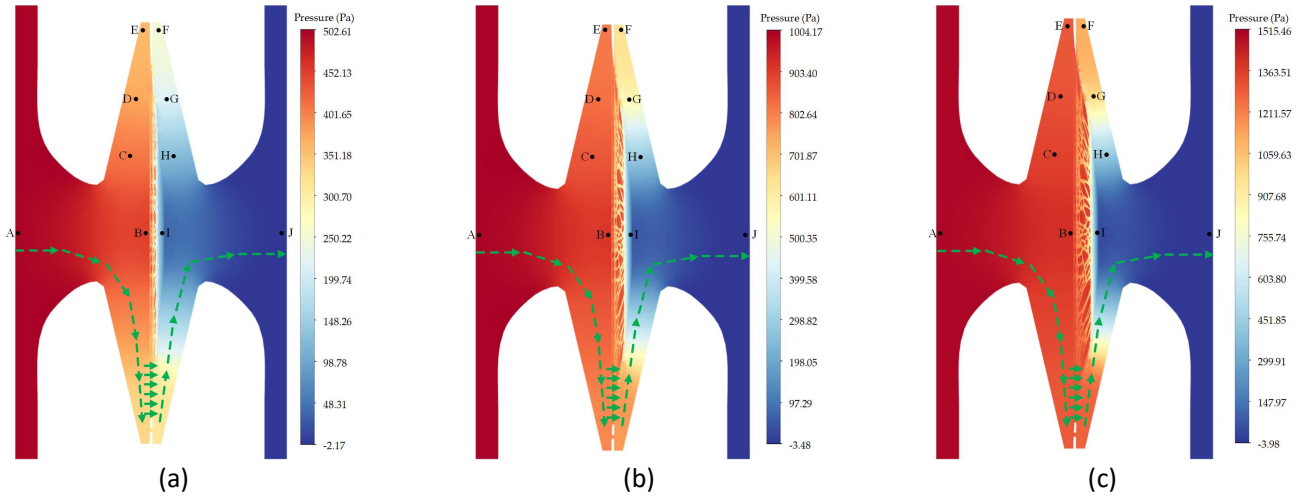

Figure 6. The influence of the fluid-solid interaction on the pressure loss in the flow path within the bordered pit. (a)500Pa, (b) 1000Pa, (c) 1500Pa.

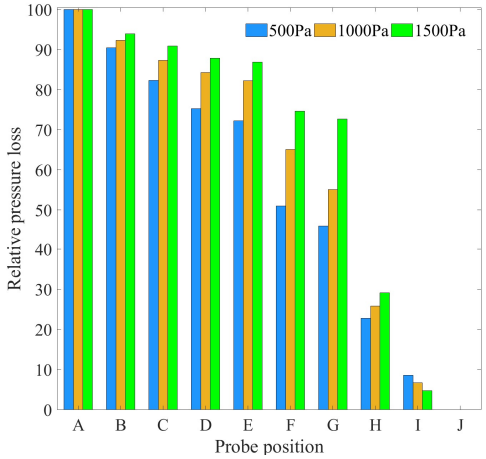

Figure 7. The relative pressure loss at the probes in the bordered pit under pressure difference 500, 1000, and 1500 Pa.

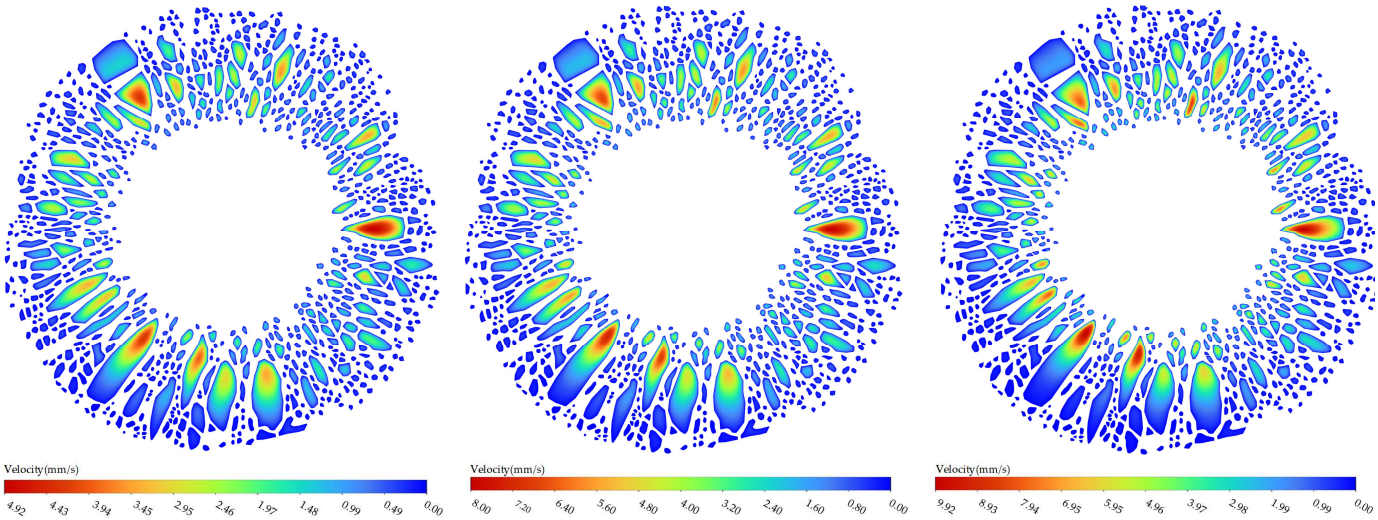

(a) (b) (c)

Figure 8. The influence of the fluid-solid interaction on the velocities in the margo pores. (a)500Pa, (b) 1000Pa, (c) 1500Pa.

When the pressure difference between tracheids linearly increased from 250 to 1750 Pa, Figure 9(a) shown that the deflection of the torus exhibited an almost linear increase from 0.0561μm to 0.3423μm. Simultaneously, a non-linear augmentation from 4.1466×10^{16}Pa·s/m3 to 8.8344×10^{16} Pa·s/m^3 in pit resistance was observed as the resistance gradient escalated with increasing torus deflection. As depicted in Figure 9(b). the fluid force on the torus-margo structure increased from 3.3099×10^{-3} μN to 19.519×10^{-3} μN with the gradient slightly decreased at higher torus deflection. When comparing the fluid force exerted on the torus and margo, it was seen that the fluid force on the torus exhibited an increase as the gradients became larger at higher torus deflection. The percentage of the fluid force exerted on the torus relative to the combined fluid force on the torus and margo experienced a rise from 39.62% to 54.68%. Additionally, as depicted in Figure 10, it was observed that the fluid force calculated in the fluid-solid interaction model was significantly lower than the simplified force with the assumption that the pressure difference between tracheids was uniformly distributed on the upstream surface of both the torus and margo, which had been employed in the solid mechanical analysis to evaluate the elastic deformation of the torus and pit structure[30,31].

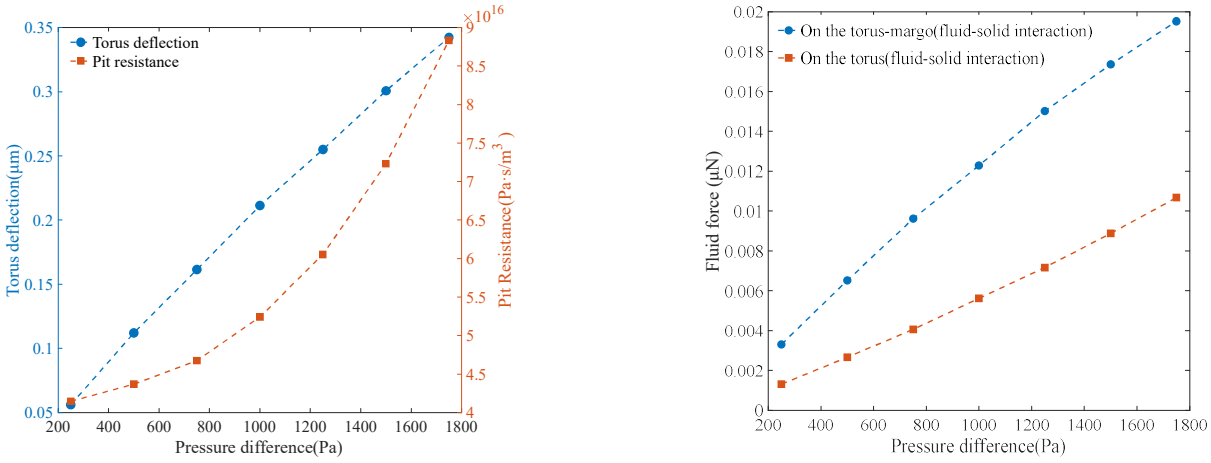

(a) (b)

Figure 9. The results of the pit under the pressure difference from 250Pa to 1750Pa, (a) The torus deflection and the pit resistance,(b)the fluid force on the torus and on the torus-margo.

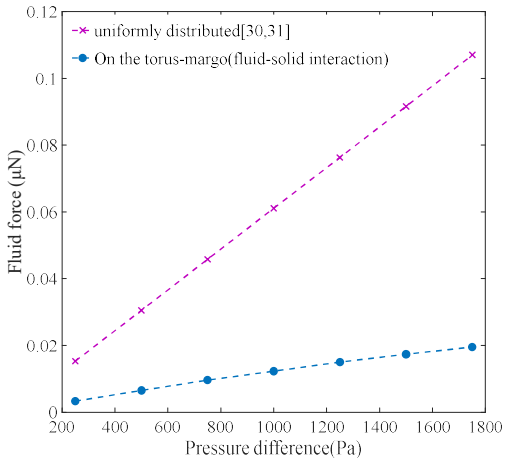

Figure 10. The comparison between the fluid force on the torus and on the torus-margo from the fluid-solid interaction model and the fluid force estimated with uniform distribution of the pressure[30,31].

Table 2 shown the geometry data and simulation results for all the pits under the pressure difference 500Pa. The torus deflection varied between 0.0689μm and 0.1704μm with an average deflection of 0.1209μm and a standard deviation of 0.0335μm, the pit resistance varied between 4.3691×10^{16}Pa·s/m^3 and 8.9994×10^{16}Pa·s/m^3 with an average resistance of 5.7373×10^{16}Pa·s/m^3 and a standard deviation of 1.3976×10^{16}Pa·s/m^3, and the resistance difference between the torus at the center position and the torus with forced deflection varied between 0.1952×10^{16}Pa·s/m^3 and 2.6020×10^{16}Pa·s/m^3 with an average area of 1.0286×10^{16}Pa·s/m^3 and a standard deviation of 0.9255×10^{16}Pa·s/m^3.

Table 2 The pit geometry and the simulation results of the pit models

No	D_{PM} (μm)	D_{TO} (μm)	L_P (μm)	S_{pore} (μm^2)	Def_{Torus} (μm)	R_{pit} (×10^{16} Pa·s/m^3)	ΔR_{pit} (×10^{16} Pa·s/m^3)
1	7.22	3.33	1.92	13.390	0.069	5.339	0.195
2	7.79	3.22	1.90	13.013	0.112	4.369	0.338
3	8.13	3.59	1.40	16.671	0.138	8.999	2.479
4	8.15	3.84	2.11	20.762	0.099	5.342	0.374
5	8.23	4.04	1.88	14.449	0.104	4.941	0.485
6	8.25	3.51	1.46	17.913	0.168	6.875	2.602
7	8.51	4.35	1.60	15.185	0.097	5.080	0.685
8	8.70	3.94	1.72	17.815	0.119	5.598	0.692
9	9.24	4.35	1.46	22.217	0.170	5.092	1.407

D_{PM}-Pit membrane diameter, D_{TO}-Torus Diameter, L_P-Pit depth, S_{pore}-Marge pore area, Def_{Torus}-Torus deflecion, R_{pit}-Pit resistance with torus deflection, ΔR_{pit}-Pit resistance with torus deflection−Pit resistance with torus placed at the pit center.

Figure 11 shown that the positive relationship between the pit diameter and the torus deflection was significant(p<0.1), and the positive relationship between the torus deflection and the resistance difference between the centered torus and the deflected torus was significant(p<0.01). Figure 12 shown the relationship between the pit diameter and the pit resistance with the deflected torus was not significant(p=0.9434), and the positive relationship between the pit diameter and the pit resistance difference was more significant (p=0.4496). Figure 13 shown that the negative relationship between the pit depth and the

pit resistance with the deflected torus was significant(p<0.1), and the negative relationship between the pit depth and the resistance difference was extremely significant (p<0.01).

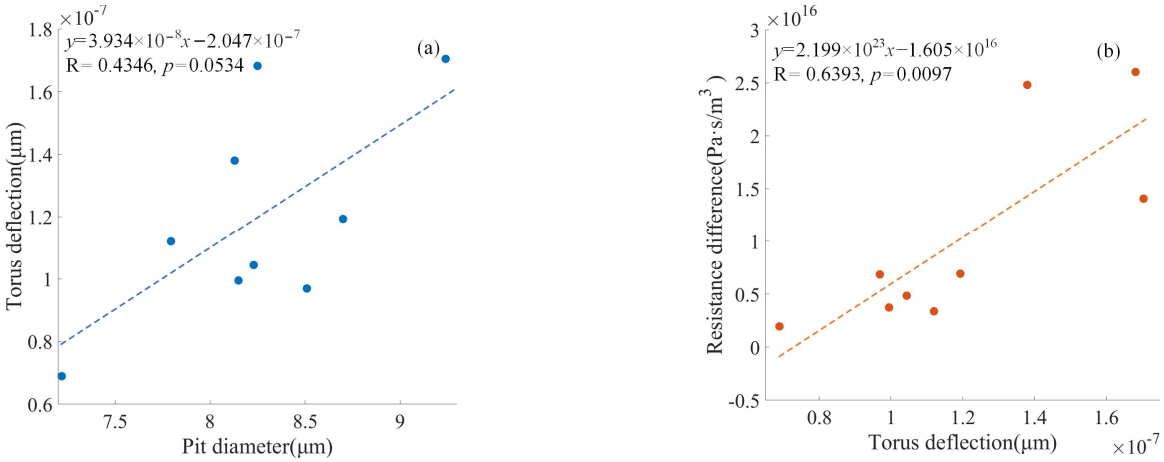

Figure 11. The influences of the pit diameter on the torus deflection and the torus deflection on the pit resistance difference. (a)the line regression between pit diameter and the torus deflection. (p<0.1) (b)the line regression between the torus deflection and the resistance difference between the centered torus and the deflected torus. (p<0.01)

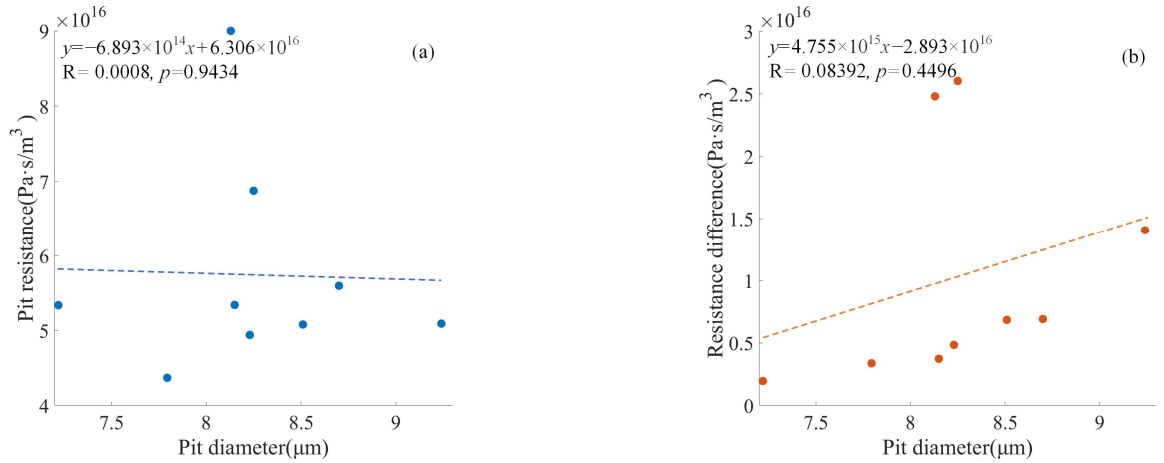

Figure 12. The influences of the pit diameter on the pit resistance with the deflected torus and the resistance difference between the centered torus and the deflected torus. (a)the line regression between the pit diameter and the torus resistance. (p=0.9434) (b)the line regression between the pit diameter and the resistance difference. (p=0.4496)

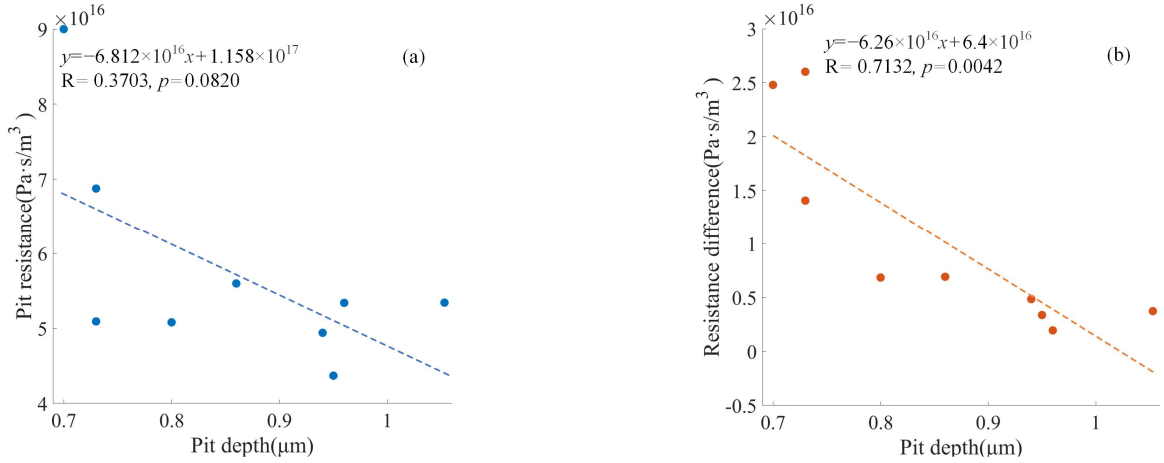

Figure 13. The influences of the pit depth on the pit resistance with the deflected torus and the resistance difference between the centered torus and the deflected torus. (a)the line regression between the pit depth and the torus resistance. (p<0.1) (b)the line regression between the pit depth and the resistance difference. (p<0.01)

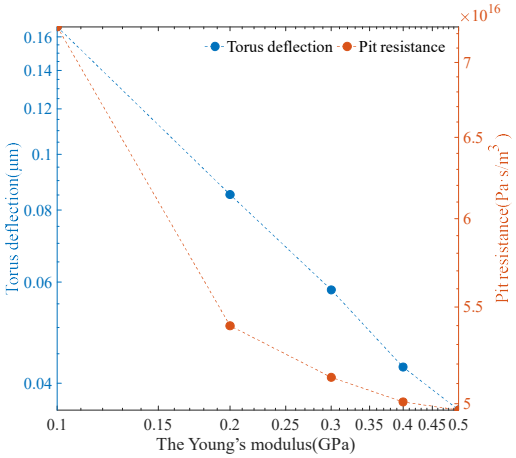

Figure 14. The influences of the Young's modulus on the torus deflection and the pit resistance in bordered pits from Platycladus orientalis.

Under the pressure difference of 250Pa, the evaluation of the effects of Young's modulus on the torus deflection and the pit resistance was conducted by implementing random one out of nine models. As shown in Figure 14, the variation in the Young's modulus value ranging from 0.1 to 0.5 GPa exhibited a significant influence on the torus deflection from 0.1666μm to 0.0359μm. Similar to the torus deflection under increasing pressure difference, the relationship between the Young's modulus and the torus deflection exhibited a nearly negative proportion. However, a non-linear reduction from 7.249×10^{16}Pa·s/m^3 to 4.968×10^{16} Pa·s/m^3 in pit resistance was observed as the Young's modulus increased.

4. Discussion

Within the context of laminar flow, which was characterized by low Reynolds numbers, the primary factor influencing flow resistance within the bordered pit was attributed to the boundaries of the flow field, namely the torus, margo, and pit border. When the torus-margo structure was initially positioned at the center, the pores in the margo could be considered as parallel channels for water flow. The Hagen-Poiseuille equation[37], utilized for the assessment of flow resistance in channel flow, established an inverse correlation between flow resistance and the fourth power of the channel's hydraulic diameter. Therefore, the larger pores in the margo were more significant in facilitating flow transportation. According to Pittermann et al. [38] and Schulte [25], it has been proposed that large pores in the margo might exert a notable influence on the hydraulic conductivity within bordered pits. Additionally, the flow resistance was further influenced by the narrow gap existed between the torus-margo structure and the pit border, particularly in proximity to the margin of the pit membrane. It was widely recognized that water flow had the ability to identify the pathway that offered the least resistance to its movement. The velocity of flow in the pores near the torus exhibited a notable increase compared to the velocity observed in the pores adjacent the margin of the pit membrane. Upon doing a comparison between the pit chamber, margo, and narrow gap, it was observed that the flow resistance in the pit chamber was found to be less influential.

The present investigation confirmed the findings of Schulte et al.[26] that broader pits reduced flow resistance compared to narrower pits. This study also discovered a negative association between pit diameter and pit resistance, although the variability in the

distribution of pores in the margo was unfavorable for the correlation significance of pit diameter on pit resistance. Based on the flow behavior in the bordered pit, the deeper pit should have lower resistance for enlarging the space within the narrow gap between the torus-margo and the pit border. Nevertheless, the correlation between the pit depth and the pit resistance was shown to be statistically insignificant. The discrepancy between the flow theory and the correlation analysis may arise due to the characteristics of the sample dataset, specifically the presence of a negative correlation between the pit diameter and the pit depth. Due to the greater impact of the margo compared to the narrow gap on pit resistance, it was possible that the correlation analysis did not accurately demonstrate the relevance of the pit depth.

To overcome the flow resistance in the bordered pit, the water had to transform energy from water pressure into water velocity. There was a significant decrease in the water pressure in the margo as well as in the narrow gap where the flow resistance predominated. When the torus was in the centered position, the pressure difference between the upstream and downstream surfaces on the torus was much higher than the difference across the margo. Hence, there was a notable link between the fluid force exerted on the torus and the diameter of the torus surface. The fluid pressure exerted on the margo exhibited dependence on the distribution of pores. The diminished correlation between fluid force and margo diameter could be attributed to the uncertainties of pore distribution. In comparison with the fluid force on the margo, the fluid force exerted on the torus was predominant of the fluid force on the torus-margo structure, despite the fact that the surface area of the margo was larger than that of the torus in all the pit models. As an increase in the pit diameter generally leaded to an increase in the surface area of the torus and the margo. The increase in pit diameter resulted in a higher fluid force acting on the torus-margo structure.

When the interaction between the fluid and the solid took effects, the deflection of the torus was significant under the pressure difference between the neighboring tracheids from 250 to 1750Pa. With the torus and margo approaching the pit border, it gave rise to narrowing the downstream gap between the torus-margo and the pit borders. Although the tours deflection enlarged the upstream gap and the margo stretching expanded the pores, the pit resistance decreased as the upstream gap was narrowed. Sperry & Tyree [17]found that the stem conductivity was dependent on flow rate among several conifers. Domec et al.[19] suggested that the apparent nonlinear reduction in a stem conductivity experiment with increasing applied pressure might be a result of the torus deflection. Due to the flow resistance in the downstream gap was higher than the resistance in the upstream gap and the margo, the pressure variation in the upstream gap and across the margo relatively decreased while the variation in the downstream gap significantly increased. As the pressure difference between tracheids increased, the fluid force on the torus and margo also increased, whereas the gradient reduced with higher torus deflection. In this preliminary study, the linear structural model of the torus and the margo was formulated, while disregarding the effects of material and geometric nonlinearity caused by significant deformation. According to the linear deformation theory, the deflection of the torus should be directly proportional to the fluid force acting on the torus-margo. However, the torus's deflection exhibited an approximately linear relationship with increasing the pressure difference. The deviation occurred due to the alteration in the distribution of force on the torus-margo. Specifically, the fluid force acting on the torus, which was more crucial for torus deflection, increased at a faster rate compared to the fluid force acting on the torus-margo. Furthermore, the pit resistance increased quickly particularly at higher pressure difference, as the flow resistance was negatively related to higher order of the hydraulic diameter. When air-seeding took place in a tracheid, the expansion of gas bubble volume was attributed to two factors: the outflow of water from the tracheid to its neighboring tracheids driven by pressure difference, and the conversion

of water into gas under negative pressure. Although the bordered pit could not prevent the water gasification under water saturation steam pressure, the non-linear increase of the pit resistance during closing the pit could obstruct the water flow and subsequent delay the bubble growth. In addition, when compared to the fluid force calculated under the assumption of uniformly distributed water pressure on the torus-margo structure[30,31], the external force derived from the fluid-solid interaction model was much smaller particularly when the torus had greater deflection. The mechanical analysis[30,31] might have underestimated the pressure difference between tracheids for pit aspiration.

When examining the flow restriction of all the pits under a pressure difference of 500Pa, it was observed that there existed an intricate relationship between the structure of the bordered pit and the pit resistance. As the torus approached the pit aperture, the narrow gap between the torus-margo and the pit border became the primary factor influencing the flow resistance within the pit. There exists a notable positive correlation between the deflection of the torus and the pit resistance difference between the centered torus and the deflected torus. The torus deflection resulted in a decrease in the impact of the margo on the pit resistance. Consequently, the relationship between the diameter of the pit and the resistance to flow became statistically insignificant. Furthermore, it was observed that the relationship between the pit depth and the pit resistance with the deflected torus exhibited a strong negative correlation, which differed from the weak association observed when the torus was positioned at the center. The findings provided empirical support for the aforementioned hypothesis that the correlation analysis might not effectively capture the significance of pit depth when the torus was positioned at the central location. The augmentation in pit diameter resulted in an increase in both the surface area of the torus-margo structure, as well as the structural flexibility of the margo. Therefore, the increase of the pit diameter promoted the torus deflection. There was a positive correlation between the resistance difference and the pit diameter, as the torus deflection increases the pit resistance. In a deeper pit, the tours needed to deflect much more to close the pit. A significant negative correlation between the resistance difference and the depth of the pit was found.

The investigation revealed that a larger pit diameter with lower flow resistance, exhibited a greater ability to regulate water flow in bordered pits. This observation took into consideration the negative correlation between pit diameter and pit resistance with the torus at the center position, as well as the positive correlation between pit diameter and resistance difference with torus deflection. Furthermore, it has been observed that an increase in pit depth with a decrease in flow resistance, reduced ability to regulate water flow in bordered pits. This observation took into consideration the negative relationship between pit depth and pit resistance with the torus at the central position, as well as the negative relationship between pit depth and the resistance difference with the torus deflection. It is noteworthy to mention that a negative correlation has been observed between the diameter of stem pits and their depth in both *Picea Mariana* [30] and *Platycladus orientalis* [31]. In contrast, a positive relationship between the diameter and depth of root pits in Picea Mariana was observed. Therefore, it was supposed that the development of bordered pits allowed for an adaptive mechanism that balanced the water transportation efficiency and the transportation adjust capacity. Given the notable variations in the geometry of bordered pits across different organs and different species [39,40], it was essential to conduct a comparative analysis among different conifer species and organs.

The behavior of the bordered pit in response to applied pressure was heavily influenced by material properties, particularly the Young's modulus. In accordance with the mechanical analysis conducted by reference [30,31], it was observed that the deflection of the torus exhibited a negative correlation with the Young's modulus. As the pit resistance was higher order of sensitivity to the torus deflection, the Young's modulus played a

considerably influential role in determining the pit resistance. When comparing the only solid analysis [30,31] to the findings of fluid-solid interaction, it was noted that the significance of Young's modulus became more important to regulate the water flow in bordered pit. Despite the importance of material properties, the availability of experimental data for the tours and margo remained limited due to the inherent challenges for measuring these microstructures. As the deformation of the margo was much higher than the torus deformation in the pit closing process, it was deemed necessary to prioritize the measurement of margo properties.

The passive regulation for the flow transportation in the bordered pit depended on pit structure, the material properties of the torus-margo, and the pressure difference between tracheids. Based on a pit structure, the passive regulation was inherently a tradeoff between the flow efficiency and regulation capability. With increasing the regulation capability, the flow resistance under lower pressure had to increase. When comparing xylem conductivities in the experiment[17-19], it was found that the difference in the performance of the passive regulation was significant between species. It was important to fully investigate the impact of flow regulation in bordered pit on the xylem network composed of tracheids and bordered pits[41]. On the other hand, the extent to which the passive regulation worked in living tree was related to the pressure gradient in the xylem, which depended on tree transpiration. Therefore, the passive regulation of bordered pit in xylem maybe represents environmental adaptation.

The present study employed a standardized modeling approach, incorporating robust mechanics theory and widely accepted engineering software, to comprehensively investigate the hydraulic characteristics of bordered pits. The investigation of fluid-solid interaction between the structure deformation and flow transportation provided insights into the flow-adjusting behavior of the torus-margo structure. The results of the simulation prompted further investigations of the microstructure of the pit, as well as the material properties of the torus and margo. In order to reduce the uncertainties of the stochasticity of pit structures on the correlation analysis, the number of pit samples should be increased in proceeding studies. To enhance the accuracy of the fluid model, the properties of the sap in stem should be measured such as density and viscosity. To improve the solid model, the material properties of the torus and margo, particularly the orientation and microstructure of the tiny fibrils in the margo. Based on the fluid-solid interaction model, to conduct a more comprehensive investigation of the propagation of air-seeding in bordered pits, it was suggested that the multiphase flow with bubble surface-tracking technique should be employed to study the growth and spread of gas bubbles.

5. Conclusion

A theoretical model was developed to investigate the phenomenon of the fluid-solid interaction in bordered pits. This model included the elastic deformation of the torus-margo structure and the flow of water transportation within the pit. Nine pit samples of *Platycladus orientalis* stems were reconstructed using scanning electron microscopy and transmission electron microscopy images. The primary sources of flow resistance in bordered pits were attributed to the pores located in the margo, the narrow space between the torus-margo and the pit border, as well as the pit chamber. In comparison to the pit chamber and the narrow gap, the resistance from the margo pores was dominant when the torus was positioned in the pit center. When the torus deviated towards the downstream pit border, the downstream narrow space was narrowed and became the prevailing factor for pit resistance at high deflection. The deflection of the torus was roughly proportional to the pressure difference, as a result of the fluid-solid interaction in bordered pits. However, the flow resistance exhibited a considerable non-linear increase as the pressure difference increased. The results presented in this work provided theoretical support for the non-linear relationship between pressure and flux in the bordered pit,

as well as for the prevention of gas bubble transit through the bordered pit during tracheid cavitation. In response to an increase in pit diameter, the pit resistance decreased with increasing pore area in the margo, meanwhile, the ability to regulate water flow was improved with increasing margo flexibility. Both pit resistance and the ability to regulate water flow in bordered pits were reduced as a result of the deepening of the pit, which created a greater gap between the torus-margo and the pit border. The Young's modulus of the margo exerted a substantial impact on the non-linear pressure-flux correlation within the bordered pit. In general, the pressure-flux correlation of water flow in bordered pits was mostly dependent on the structure of the pit and the material properties of the torus and margo.

Author Contributions: Conceptualization, X.P.; methodology, X.P. and S.W.; software, W.Y.; validation, X.L.; resources, L.Q.; data curation, J.Z.; writing—original draft preparation, W.Y.; writing—review and editing, X.P.; visualization, W.X. All authors have read and agreed to the published version of the manuscript.

Funding: This research was funded by the National Natural Science Foundation of China (No. 32001286) and the Fundamental Research Funds for the Central Universities (No. 2572021BF06).

Data Availability Statement: Data will be made available on request.

Conflicts of Interest: The authors declare no conflict of interest.

References

1. Kiorapostolou, N.; Camarero, J.J.; Carrer, M.; Sterck, F.; et al. Scots pine trees react to drought by increasing xylem and phloem conductivities. *Tree Physiol*. **2020**, *40*, 774-781.
2. Song, Y.; Poorter, L.; Horsting, A.; Delzon, S.; et al. Pit and tracheid anatomy explain hydraulic safety but not hydraulic efficiency of 28 conifer species. *J. Exp. Bot.* **2022**, *73*, 1033-1048.
3. Sviderskaya, I.V.; Vaganov, E.A.; Fonti, M.V.; et al. Isometric scaling to model water transport in conifer tree rings across time and environments. *J. Exp. Bot.* **2021**, *72*,2672-2685.
4. Johnson, D.M.; Katul, G.; Domec, J.C. Catastrophic hydraulic failure and tipping points in plants. *Plant Cell Environ.* **2022**, *45*, 2231-2266.
5. Venturas, M.D.; Sperry, J.S.; Hacke, U.G. Plant xylem hydraulics: what we understand, current research, and future challenges. *J. Integr. Plant. Biol.* **2017**, *59*, 356-389.
6. Domec, J.C.; Lachenbruch, B.; Meinzer, F.C. Bordered pit structure and function determine spatial patterns of air-seeding thresholds in xylem of Douglas-fir (Pseudotsuga menziesii; Pinaceae) trees. *Am. J. Bot*. **2006**, *93*, 1588–1600.
7. Sperry, J.S.; Hacke, U.G.; Pittermann, J. Size and function in conifer tracheids and angiosperm vessels. *Am. J. Bot.* **2006**, *93*, 1490–1500.
8. Schoonmaker, A.L.; Hacke, U.G.; Landh€ausser, S.M.; et al. Hydraulic acclimation to shading in boreal conifers of varying shade tolerance. *Plant Cell Environ.* **2010**, *33*, 382–393.
9. Chapman, D.C.; Rand, R.H.; Cooks, J.R. A hydrodynamical model of bordered pits in conifer tracheids. *J. Theor. Biol*. **1977**, *67*, 11-24.
10. Bouche, P.S.; Jansen, S.; Cochard, H.H.; et al. Embolism resistance of conifer roots can be accurately measured with the flow-centrifuge method. *J. Plant. Hydraul.* **2015**, *2*, e002.
11. Maruta, E.; Yazaki, K.; Ogasa, M.Y. Pit aspiration causes an apparent loss of xylem hydraulic conductivity in a subalpine fir (Abies mariesii Mast) overwintering at the alpine timberline. *Tree Physiol.* **2022,** *42*, 1228-1238.
12. Jansen, S.; McAdam, S. Pits with aspiration explain life expectancy of a conifer species. *P. Nayl. A. Sci*. **2019,** 116, 14794-14796.

13. Gaylord, M.L.; Kolb, T.E.; McDowell, N.G. Mechanisms of piñon pine mortality after severe drought: a retrospective study of mature trees. *Tree physiol*. **2015,** *35*, 806-816.
14. Roskilly, B.; Keeling, E.; Hood, S.; Giuggiola, A.; Sala A. Conflicting functional effects of xylem pit structure relate to the growth-longevity trade-off in a conifer species. *P. Nayl. A. Sci.* **2019,** *116*, 15282-15287.
15. Mayr, S.; Kartusch, B.; Kikuta, S.; et al. Evidence for air-Seeding: watching the formation of embolism in conifer xylem. *J. Plant. Hydraul.* **2014**, *1*, e004.
16. Savidge, R.A. Cell biology of bordered-pit formation in balsam-fir trees. *Botany*. **2014**, *92*, 495-511.
17. Sperry, J.S.; Tyree, M.T. Water-stress-induced xylem embolism in three species of conifers. *Plant Cell Environ*. **1990**, *13*, 427-436.
18. Cochard, H.; Holtta, T.; Herbette, S.; et al. New insights into the mechanisms of water-stress-induced cavitation in conifers. *Plant Physiol*. **2009**, *151*, 949-954.
19. Domec, J.C.; Meinzer, F.C.; Lachenbruch, B.; et al. Dynamic variation in sapwood specific conductivity in six woody species. *Tree Physiol*. **2007**, *27*, 1389-1400.
20. Zelinka, S. L.; Bourne K. J.; Hermanson J.C.; et al. Force–displacement measurements of earlywood bordered pits using a mesomechanical tester. *Plant Cell Environ*, **2015**, *38*, 2088-2097.
21. Winbourne, J.B.; Jones, T.S.; Garvey, S.M.; et al. Tree transpiration and urban temperatures: current understanding, implications, and future research directions. *BioScience*. **2020**, *70*, 576-588.
22. Chuang, Y.L.; Oren, R.; Bertozzi, A.L.; et al. The porous media model for the hydraulic system of a conifer tree: Linking sap flux data to transpiration rate. *Ecol Model*. **2006**, *191*, 447-468.
23. Lancashire, J.R.; Ennos, A.R. Modelling the hydrodynamic resistance of bordered pits. *J. Exp. Bot*. **2002**, *373*, 1485–1493.
24. Valli, A.; Koponen, A.; Vesala, T.; et al. Simulations of water flow through bordered pits of conifer xylem. *J. Stati. Phys*. **2002**, *107*, 121-142.
25. Schulte, P.J. Computational fluid dynamics models of conifer bordered pits show how pit structure affects flow. *New Phytol*. **2012**, *193*, 721-729.
26. Schulte, P.J.; Hacke, U.G.; Schoonmaker, A.L. Pit membrane structure is highly variable and accounts for a major resistance to water flow through tracheid pits in stems and roots of two boreal conifer species. *New Phytol*. **2015,** *208*, 102-113.
27. Sperry, J.S.; Hacke, U.G. Analysis of circular bordered pit function I. Angiosperm vessels with homogenous pit membranes. *Am. J. Bot*. **2004**, *91*, 369–385.
28. Tixier, A.; Herbette, S.; Jansen, S.; et al. Modelling the mechanical behaviour of pit membranes in bordered pits with respect to cavitation resistance in angiosperms. *Ann. Bot*. **2014**, *114*, 325–334.
29. Hacke, U.G.; Sperry, J.S.; Pittermann, J. Analysis of circular bordered pit function II. Gymnosperm tracheids with torus-margo pit membranes. *Am. J. Bot*. **2004**, *91*, 386–400.
30. Schulte, P.J.; Hacke, U.G. Solid mechanics of the torus–margo in conifer intertracheid bordered pits. *New Phytol.* **2020**, *229*, 1431–1439.
31. Xia, P.; Gu, J.; Song, W.; Xie, L.; Wu, Y.; Zhang, H.; Li, Q. Contact Mechanics between Torus and Pit Border for Developing Air-Seeding Seal in Aspirated Bordered Pits. *Forests*. **2023**, *14*, 2324.
32. Schetz, J.A.; Fuhs, A.E. *Fundamentals of fluid mechanics.* John Wiley & Sons, **1999**.
33. Wesseling, P. *Principles of computational fluid dynamics*. Springer Science & Business Media, **2009**.
34. Sadd, M.H. *Elasticity: Theory, Applications, and Numerics*; Academic Press: Cambridge, MA, USA, **2009**.
35. Larson, M.G.; Bengzon, *F. The Finite Element Method: Theory, Implementation, and Applications*; Springer Science and

Business Media: New York, NY, USA, **2013**.
36. Richter, T. *Fluid-structure interactions: models, analysis and finite elements*. Vol. 118. Springer, **2017**.
37. Woodruff, D,R. The impacts of water stress on phloem transport in Douglas-fir trees. *Tree physiol*. **2014**, *34*, 5-14.
38. Pittermann, J.; Choat, B.; Jansen, S.; et al. The relationships between xylem safety and hydraulic efficiency in the Cupressaceae: the evolution of pit membrane form and function. *Plant Physiol.* **2010**, *153*, 1919–1931.
39. Hacke, U. G.; Jansen, S. Embolism resistance of three boreal conifer species varies with pit structure. *New Phytol*. **2009**, *182*, 675-686.
40. Bouche, P.S.; Larter, M.; Domec, J.C.; et al. A broad survey of hydraulic and mechanical safety in the xylem of conifers. *J. Exp. Bot.* **2014**, *65*, 4419–4431.
41. Irina, V.Sviderskaya.; Eugene, A.Vaganov.; Marina, V.Fonti. Isometric scaling to model water transport in conifer tree rings across time and environments. *J. Exp. Bot.* **2021**, *72*, 2672–2685.

Disclaimer/Publisher's Note: The statements, opinions and data contained in all publications are solely those of the individual author(s) and contributor(s) and not of MDPI and/or the editor(s). MDPI and/or the editor(s) disclaim responsibility for any injury to people or property resulting from any ideas, methods, instructions or products referred to in the content.